# A fluid–structure interaction framework for mechanical aortic valves: analyzing the effects of valve design and aortic curvature on hemodynamics

# A fluid–structure interaction framework for mechanical aortic valves: analyzing the effects of valve design and aortic curvature on hemodynamics

IOP Publishing Med. Eng. Phys. 147 (2026) 015008 https://doi.org/10.1088/1873-4030/ae1e76

Medical Engineering & Physics

IPEM Institute of Physics and Engineering in Medicine



PAPER

# A fluid–structure interaction framework for mechanical aortic valves: analyzing the effects of valve design and aortic curvature on hemodynamics

**Mariachiara Arminio[1], Dario Carbonaro[1], Valentina Mazzi[1], Karol Calò[1], Rodrigo Paz[2,3], Facundo Del Pin[2], Diego Gallo[1], Umberto Morbiducci[1] and Claudio Chiastra[1,*]**

[1] Polito[BIO]Med Lab, Department of Mechanical and Aerospace Engineering, Politecnico di Torino, Turin, Italy
[2] ANSYS Inc., Livermore, CA, United States of America
[3] IMIT, CONICET, National Council for Scientific and Technical Research, Resistencia, Argentina
[*] Author to whom any correspondence should be addressed.

**E-mail:** claudio.chiastra@polito.it, mariachiara.arminio@polito.it, dario.carbonaro@polito.it, valentina.mazzi@polito.it, karol.calo@polito.it, Rodrigo.Paz@ansys.com, Facundo.DelPin@ansys.com, diego.gallo@polito.it and umberto.morbiducci@polito.it

OPEN ACCESS

RECEIVED
15 May 2025

REVISED
26 August 2025

ACCEPTED FOR PUBLICATION
15 October 2025

PUBLISHED
9 January 2026



**Keywords:** heart valve prosthesis, mechanical aortic valves, bileaflet valves, *in silico* medicine, fluid–structure interaction

Supplementary material for this article is available online

## Abstract

Aortic mechanical heart valves (MHVs) have been implanted for decades to treat aortic valve disease and remain a viable option when valve durability is prioritized. However, the non-physiological hemodynamics induced by MHVs may lead to adverse clinical outcomes. Fluid–structure interaction (FSI) simulations enable the analysis of the biomechanical interaction between MHVs and blood flow. This study presents a strongly coupled, boundary-fitted FSI framework for aortic MHVs, used to assess the impact of MHV design and aortic curvature on hemodynamics. Nine simulation scenarios were investigated, considering three commercially available MHVs and three idealized aortic geometries (one straight and two curved models). Overall, the framework proved to provide results for flow-rate waveforms, velocity fields, and leaflet kinematics aligning well with previous experimental and computational studies. The framework highlighted that: (i) MHV design influences velocity fields and large-scale vorticity transport in the aorta, with systolic differences among the three devices of up to 41% and 133% in average swirling strength and stretching, respectively; (ii) the straight aortic model underestimates systolic swirling strength (up to 56%) and stretching (up to 91%) compared to curved models. This FSI framework can support MHV development by analyzing different device designs and anatomical scenarios.

## 1. Introduction

Aortic valve replacement is an established clinical practice for treating severe aortic valve disease, involving the implantation of either a surgical or a transcatheter prosthesis (Head *et al* 2017, Otto *et al* 2020). Aortic mechanical heart valves (MHVs) featuring rigid leaflets represent the preferred option for patients under 50 and were used for 30% of aortic valve replacement procedures in the United States between 2009 and 2018 (Otto *et al* 2020, Hiltner *et al* 2022). The clinical outcomes of MHVs are markedly influenced by the non-physiological hemodynamics they induce. In particular, flow patterns downstream of aortic MHVs are characterized by altered vorticity transport and elevated shear stress, which promote platelet activation and aggregation thereby increasing the risk of thromboembolic events (Bluestein *et al* 2000, Yoganathan *et al* 2004, Sotiropoulos *et al* 2016, Zakaria *et al* 2017).

The hemodynamics of aortic MHVs has been extensively investigated through both experimental and computational approaches (Sotiropoulos *et al* 2016, Abbas *et al* 2022, Arminio *et al* 2024). In accordance

with international standards (International Organization for Standardization 2021), *in vitro* studies commonly utilize pulse duplicator systems to assess hydrodynamic performance and visualize flow fields. *In silico* models offer an effective tool for the biomechanical assessment of MHVs, complementing experimental tests by providing high-resolution four-dimensional flow analyses and enabling the exploration of various operating conditions with reduced time and costs compared to *in vitro* investigations (Arminio *et al* 2024). Specifically, fluid–structure interaction (FSI) simulations allow for a comprehensive evaluation of MHV biomechanics by capturing the complex interaction between the valve and blood flow (Sotiropoulos and Borazjani 2009, Arminio *et al* 2024).

Numerous studies have developed FSI frameworks to analyze aortic MHV hemodynamics, but relatively few have employed simulations to compare different MHV designs (Arminio *et al* 2024). Additionally, the majority of FSI models have replicated experimental set-ups involving idealized, straight aortic geometries. This simplification may limit the capability of FSI simulations to replicate the *in vivo* hemodynamics of MHVs. In this context, studies by Borazjani *et al* (2010) and Annerel *et al* (2015) employed FSI simulations to evaluate MHVs implanted in both idealized (straight) and patient-specific aortic geometries. Their findings highlighted differences in flow jet characteristics and vortex shedding behavior between the two aortic models, underlining the importance of anatomical realism in MHV hemodynamic investigation. This is further supported by a study by Kuan *et al* (2014), which involved FSI simulations of a MHV implanted in both straight and curved idealized aortic models, revealing differences in flow patterns within the hinge regions.

This study presents an FSI framework for simulating aortic MHVs, used here to investigate the impact of both MHV design and aortic curvature on hemodynamics. After comparison against findings from a previous study that included both experimental and computational analyses (Nobili *et al* 2008), the FSI framework was applied to investigate the hemodynamic behavior of three commercially available MHVs implanted in an idealized straight aortic model. Additionally, the framework was used to assess the effects of aortic curvature by simulating the three MHV designs within idealized aortic models featuring different curvature.

## 2. Methods

### 2.1. MHV models

Three geometric models of aortic bileaflet MHVs with nominal size of 27 mm were created using SolidWorks (Dassault Systèmes, FR). The MHV models were designed to replicate three commercially available MHVs: the St. Jude Hemodynamic Plus (HP) (Abbott Laboratories, IL, USA), the On-X (Artivion, GA, USA), and the Carbomedics (CM) Standard (Corcym Srl, IT) (figure 1(A), upper panel). Shape and dimensions were retrieved from manufacturer datasheets. To reduce computational costs, the hinge mechanism connecting MHV leaflets to the housing was neglected and the blocking mechanism of the hinge was replaced by a frictionless angular constraint on leaflet rotation (De Tullio *et al* 2009). Leaflet maximum opening angles were set to 85°, 90° and 78° with respect to MHV plane for the HP, On-X and CM valves, respectively, based on manufacturer datasheets and previous studies (Nobili *et al* 2008, Hatoum *et al* 2020).

### 2.2. Aortic models

A model replicating the aortic root of the ViVitro Pulse Duplicator system (ViVitro Labs Inc., BC, CA) was reconstructed in HyperMesh (Altair Engineering, MI, USA) (Nobili *et al* 2008). In this model, the three sinuses of Valsalva were shaped as semispherical domes with 120° anatomical symmetry (Nobili *et al* 2008). An 80 mm-long ventricular conduit was positioned upstream of the aortic root model. To examine the impact of the aortic curvature on MHV hemodynamics, one straight and two curved conduits were placed downstream of the aortic root. The resulting aortic model with a straight aortic conduit is hereafter referred to as 'straight', while the models with curved aortic conduits are referred to as CU1 and CU2 (figure 1(A), lower panel). The aortic conduits (30 mm diameter) were generated in SolidWorks, with the geometry of the curved conduits derived from morphometric data (Sugawara *et al* 2008, Redheuil *et al* 2011). Specifically, the conduit used in model CU1 features an arch width of 73.3 mm, an arch height of 41.4 mm, and an ascending aorta length of 75.6 mm. For model CU2, the corresponding values are 62.1 mm, 35.5 mm, and 57.6 mm, respectively. These dimensions were selected based on data reported by Redheuil *et al* (2011) and Sugawara *et al* (2008), which provide age-specific values for arch width, arch height, and ascending aorta length for patients aged 50–59 (CU1) and 30–39 (CU2). However, due to the large anatomical variability, models CU1 and CU2 should not be considered strictly representative of these age groups. The resulting arch height-to-width ratios were 0.565 for CU1

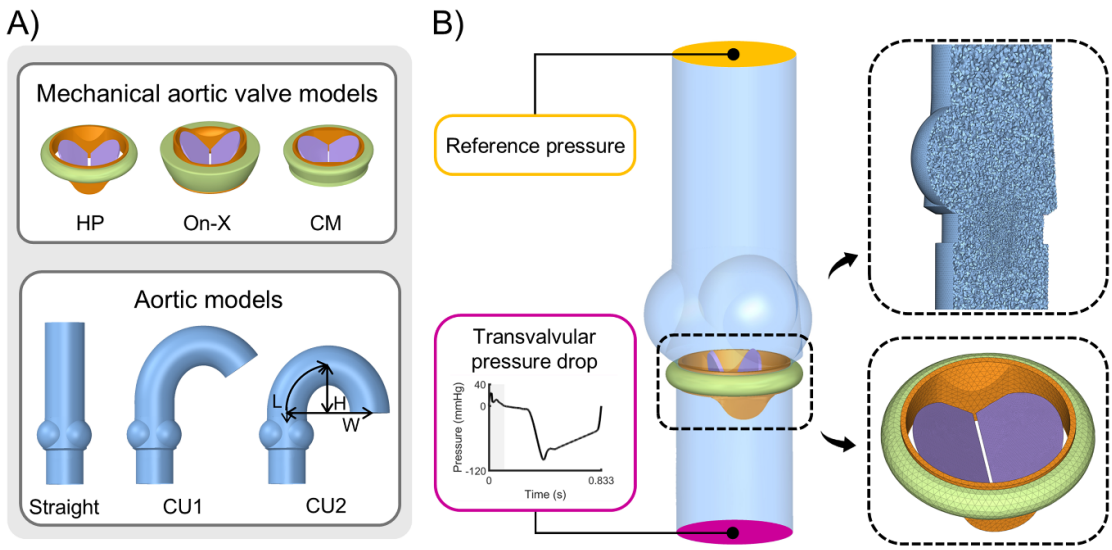


**Figure 1.** Geometric models and boundary conditions for fluid–structure interaction simulations: (A) Geometric models of the Hemodynamic Plus (HP), On-X and Carbomedics Standard (CM) mechanical heart valves (MHVs) (leaflets in purple, housing in orange, and sewing cuff in green) and the aortic conduit (W: arch width; H: arch height; L: ascending aorta length); the straight aortic model replicates the aortic root of a ViVitro Pulse Duplicator system. (B) Fluid–structure interaction MHV model: Hemodynamic Plus valve assembled with the straight aortic conduit model, including inlet and outlet boundary conditions, along with magnified images of the meshes. The gray box in the transvalvular pressure drop graph indicates the period of the cardiac cycle during which the pressure drop is positive. For improved visualization, the aortic and fluid domain representations depict only portions of the complete geometry.

and 0.572 for CU2. In the absence of age-related data on aortic torsion, a twist angle of 24.2° was adopted for both curved models (Conti *et al* 2010), while the aortic tilt angle was not included (Conti *et al* 2010). The outflow sections of the straight and curved aortic conduits were positioned to ensure the same systolic flow rate across the three models when subjected to an identical pressure drop between the inflow and outflow sections. This resulted in the outflows being positioned at an equal curvilinear distance of 110 mm distal to the sinotubular junction.

### 2.3. Simulation domain and discretization

The simulation domain consisted of the fluid volume with embedded MHV leaflets and was obtained subtracting MHV housing and cuff from the aortic model (figure 1(B)). The aortic wall was assumed to be rigid and fixed over time. The MHV leaflet movement was modeled as a rigid body rotation. The MHV orientation and implantation height within the aortic model reproduced the configuration adopted by Nobili *et al* (2008), with one of MHV leaflets facing the right coronary sinus, corresponding to the orientation recommended for maximizing left coronary flow (Kleine *et al* 2002).

The domain was meshed using HyperMesh in conjunction with LS-DYNA (Ansys Inc., PA, USA). Specifically, the MHV housing and cuff were discretized using tetrahedral elements with a size of 1 mm, while MHV leaflets were discretized with triangular shell elements with a size of 0.25 mm (figure 1(B)). The fluid domain was meshed with approximately 5 million tetrahedral elements (figure 1(B)). Throughout the simulation, the fluid domain was automatically remeshed by LS-DYNA ICFD solver to prevent element quality deterioration or inversion due to MHV leaflet rotation. The element sizes were determined based on the mesh independence study detailed in the supplementary data.

To activate the fluid-MHV leaflets interaction, fluid counterparts for MHV leaflets were embedded in the fluid domain. The geometry and the mesh of the 'fluid' leaflets were identical to those of the structural leaflets, except for a gap along the edges of the 'fluid' leaflets, modeled to prevent them from contacting each other and the wall boundaries during MHV closure. The gap size was set to 0.15 mm along the opposing sides of the leaflets and 0.30 mm elsewhere. To prevent flow through the artificial gap, a gap closure treatment was activated in the ICFD solver (Huang *et al* 2021).

### 2.4. Material properties

MHV leaflets were modeled as rigid, with densities of 2200 kg $m^{-3}$, 2100 kg $m^{-3}$, and 2000 kg $m^{-3}$ for the HP, On-X and CM valves, respectively (Nobili *et al* 2008, Annerel *et al* 2015, Sadipour *et al* 2020). Blood was modeled as homogeneous, incompressible, Newtonian fluid, with a density of 1060 kg $m^{-3}$ and a viscosity of 3.7 cP (Nobili *et al* 2007, 2008).

### 2.5. Boundary conditions

To enable comparison of results with those reported by Nobili *et al* (2008), a Neumann boundary condition was applied to the inflow and outflow sections of the fluid domain. Specifically, a transvalvular pressure drop and a zero reference pressure were prescribed at the inflow and outflow sections, respectively. The systolic pressure drop was the same as in Nobili *et al* (2008), and the diastolic pressure drop was derived from Wu *et al* (2019). The resulting pressure drop curve (with a period of 0.833 s, figure 1(B)) complies with ISO 5840:2021 standards regarding peak differential pressure across a closed valve for *in vitro* testing of surgical aortic valve substitutes (International Organization for Standardization 2021). The no-slip boundary condition was imposed at the fluid wall and fluid–structure interface.

### 2.6. Solver set-up

Simulations of the two-way interaction between MHV leaflets and blood were conducted by coupling LS-DYNA ICFD and structural implicit finite element solvers. Technically, the governing equations of fluid motion were approximated with a boundary-fitted method—arbitrary Lagrangian-Eulerian approach, which effectively manages high mesh deformations and accurately represents the pressure discontinuity between aortic and ventricular sides (Oliveira *et al* 2024). The variational multiscale (VMS) method combined with the orthogonal subgrid stabilization (OSS) technique was used to prevent numerical instabilities (Codina *et al* 2004, Bazilevs *et al* 2007). A strong coupling between the fluid and structural domains was adopted, thereby ensuring results convergence at the fluid–structure interface (Oliveira *et al* 2024).

Simulation time step was fixed to $10^{-4}$ s (Zhou *et al* 2023). Two cardiac cycles were simulated to guarantee cycle-to-cycle reproducibility (see supplementary data), and results were extracted from the second one.

### 2.7. Numerical experiments

#### *2.7.1. Comparison with previous experimental and numerical results*

To support the reliability of the proposed FSI framework, the results for the HP valve in a straight aortic model, specifically the flow-rate waveform, leaflet kinematics, and peak systolic velocity field, were compared with both experimental and numerical data from Nobili *et al* (2008). To ensure consistency, the same geometric model, material properties, rheological characteristics as in Nobili *et al* (2008) were used, and the systolic transvalvular pressure drop from the same study (Nobili *et al* 2008) was prescribed as a boundary condition. The ventricular and aortic conduit lengths were adjusted so that the inflow and outflow were positioned at the same distance from the valve as the pressure sensors in the study by Nobili *et al* (2008).

#### *2.7.2. Impact of MHV design and aortic curvature*

To analyze the impact of MHV design and aortic curvature on MHV-related hemodynamics, nine scenarios were simulated, where each valve model was combined with the three aortic models. Results were analyzed in terms of velocity fields, large-scale vorticity transport, coherence of large-scale fluid structures and effective orifice area (EOA), as detailed in section 2.8.

### 2.8. Analysis of MHV hemodynamics

Vortex structures were analyzed using the $\lambda_2$ criterion for vortex identification. The $\lambda_2$ criterion enables vortex visualization by identifying vortex cores (Jeong and Hussain 1995), and it is based on the calculation of the eigenvalue $\lambda_2$ from the three eigenvalues of tensor $\mathbf{S}^2 + \mathbf{\Omega}^2$ (sorted so that $\lambda_1 \geqslant \lambda_2 \geqslant \lambda_3$), where $\mathbf{S}$ and $\mathbf{\Omega}$ are the symmetric and the antisymmetric parts of the velocity gradient tensor, respectively.

Furthermore, vorticity transport was analyzed in terms of stretching and swirling strength. Vorticity stretching measures the rate at which the vorticity vector is amplified due to the deformation and tilting of vortex tubes in the flow field. For an incompressible fluid, it can be quantified from the vorticity transport equation:

$$\frac{\partial \boldsymbol{\omega}}{\partial t} + (\boldsymbol{u} \cdot \nabla)\,\boldsymbol{\omega} = (\boldsymbol{\omega} \cdot \nabla)\,\boldsymbol{u} + \nu \Delta \boldsymbol{\omega} \tag{1}$$

where $\boldsymbol{u}$ and $\boldsymbol{\omega}$ are the velocity and the vorticity vectors, respectively, and $\nu$ is the kinematic viscosity. The first term at second member in equation (1), the so-called stretching term, represents the rotational acceleration resulting from the rate-of-strain parallel (or anti-parallel) to the vorticity vector (Petitjeans 2003, Corso and Obrist 2024).

The swirling strength quantifies the local swirling rate inside a vortex, and it is defined as the imaginary part of the complex conjugate eigenvalues of the velocity gradient tensor (Zhou *et al* 1999).

Volume-averaged swirling strength and stretching were computed over the entire fluid domain as well as over the aortic segment distal to the sinotubular junction. Volume-averaged vorticity-based quantities were also averaged over the entire systole.

Large-scale hemodynamic coherence was evaluated applying the recently proposed '*one-to-all*' network approach to fluid velocity data (Calò *et al* 2023a, 2023b, 2024). Specifically, the impact of MHV design and aortic curvature on the coherence of large-scale fluid structures was assessed in terms of length of persistence of the correlation between the flow-rate waveform at the sinotubular junction and the local fluid axial velocity waveforms distal to the junction, quantified through the average weighted curvilinear distance (AWCD) (Calò *et al* 2023a, 2023b, 2024). The approach is based on describing the aorta as a network comprising a reference node located at the sinotubular-junction cross-section linked with $N$ nodes distal to the sinotubular junction. The reference node is characterized by the flow-rate waveform $Q(t)$, while each distal node is characterized by the blood axial velocity waveform $u_{\mathrm{ax},i}(t)$. For each distal node, the Pearson correlation coefficient between $Q(t)$ and $u_{\mathrm{ax},i}(t)$ is used as a measure of the dynamic similarity between the driving flow rate and the nodal axial velocity waveforms along the cardiac cycle. Consequently, the AWCD is calculated as:

$$\mathrm{AWCD} = \frac{1}{l}\frac{1}{N}\sum_{i=1}^{N} R_i^Q \cdot s_{\mathrm{STJ}-i} \tag{2}$$

where $l$ is the length of the aorta, $N$ is the number of nodes in the aortic fluid domain, $R_i^Q$ is the correlation coefficient between $Q(t)$ and $u_{\mathrm{ax},i}(t)$ waveforms, and $s_{\mathrm{STJ}-i}$ is the difference between the curvilinear abscissa values defining the cross-section containing node $i$ and the sinotubular junction cross-section.

Finally, the EOA of MHVs was computed according to ISO 5840:2021 (International Organization for Standardization 2021) as:

$$\mathrm{EOA} = \frac{q_{v_{\mathrm{RMS}}}}{51.6 \times \sqrt{\Delta p/\rho}} \tag{3}$$

where the EOA is expressed in $\mathrm{cm}^2$, $q_{v_{\mathrm{RMS}}}$ is the root mean square forward flow during the positive differential pressure period (expressed in ml $\mathrm{s}^{-1}$), $\Delta p$ is the mean pressure difference (measured during the positive differential pressure period and expressed in mmHg), and $\rho$ is the density of the test fluid expressed in g $\mathrm{cm}^{-3}$.

## 3. Results

### 3.1. FSI model comparison with literature data

The flow-rate waveform calculated from the FSI simulation replicating the experiment for the HP valve in a straight aortic model reported in Nobili *et al* (2008) compared satisfactorily with the experimental flow-rate waveform measured in that study (figure 2(A)). Minor differences were related to an underestimation of the experimental peak flow rate (∼6%) and of the stroke volume (∼7%), as well as to the presence of oscillations shortly after MHV closure. MHV leaflet kinematics was also in good agreement with experimental and numerical results by Nobili *et al* (2008) (figure 2(B)), with the leaflet opening angle reaching the nominal value of 85°, as in the computational analysis in the reference study. The leaflet closing time was 0.3224 s and matched experimental data (0.3324 ± 0.0058 s) (Nobili *et al* 2008). Additionally, a qualitative comparison of the axial velocity field at peak systole between the proposed FSI model and that of Nobili *et al* (2008) (figure 2(C)) revealed a close similarity, with comparable velocity distributions in the three forward flow jets and in the low-velocity recirculation region in the aortic sinus.

To further support the reliability of the proposed FSI model, velocity magnitude and swirling strength results (figure 3) were qualitatively compared with previous studies (Dasi *et al* 2007, Ge and Sotiropoulos 2007, Abbas *et al* 2025). In agreement with the literature, vortex structures emerged at the edges of the MHV housing, as well as near the upper edge of the sinuses as the valve opened (figures 3(A) and (B)) (Dasi *et al* 2007). The $\lambda_2$ criterion also revealed vortex shedding in the wake of the MHV leaflets, as expected. As previously reported (Dasi *et al* 2007, Ge and Sotiropoulos 2007), these shed vortices interacted with the downstream vortex ring formed beyond the MHV housing (figures 3(B) and (C)). Flow recirculation characterized by low velocity magnitude was observed within the aortic

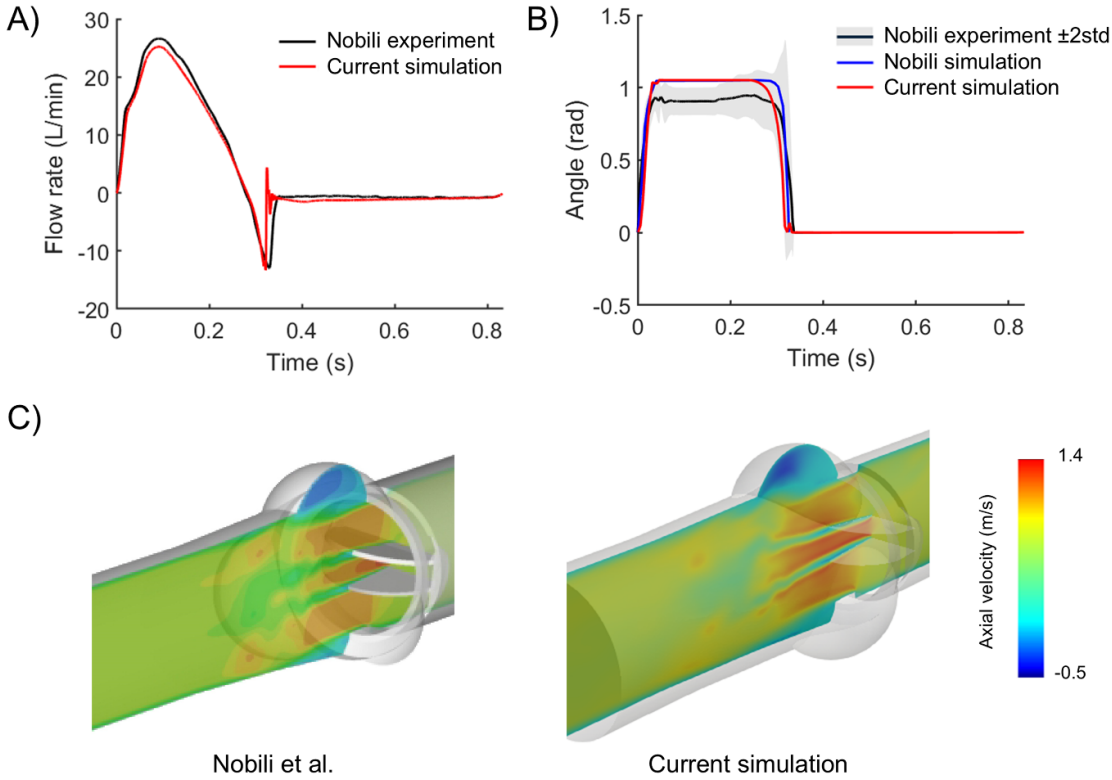


**Figure 2.** Comparison between the proposed FSI framework and the results reported by Nobili *et al* (2008): (A) flow-rate waveform, (B) leaflet kinematics, and (C) axial velocity color maps on a longitudinal section at peak systole for the proposed fluid–structure interaction model (Hemodynamic Plus valve in the straight aortic model) and from Nobili *et al* (2008). The left picture of panel C is adapted from Nobili *et al* (2008), Copyright 2008, with permission from Elsevier.

sinuses, consistent with earlier findings (Abbas *et al* 2025). These flow features result from the combined effects of sinus geometry, forward flow, and the bileaflet configuration of the MHV. Additionally, the three systolic jets generated by the valve diffused rapidly downstream of the valve annulus, in line with previous observations (Abbas *et al* 2025). During the rapid deceleration phase of systole, large coherent vortex structures broke down into smaller ones, filling the aortic root and proximal conduit (figure 3(D)) (Dasi *et al* 2007, Abbas *et al* 2025).

### 3.2. Impact of MHV design on hemodynamics

The cardiac output (CO) values for the simulations of the three MHVs assembled with the straight aortic model are reported in table 1. The HP valve simulation was characterized by the highest CO (4.62 l $min^{-1}$), while the CM valve simulation was characterized by the lowest (3.44 l $min^{-1}$). Color maps of velocity magnitude, $\lambda_2$ criterion and swirling strength iso-surfaces for the three MHVs at peak systole are presented in figure 4, depicting the three flow jets and flow recirculation in the aortic sinus upstream of the straight aortic conduit. For completeness, visualizations of velocity magnitude on axial cross-sections and of vorticity stretching are provided in figures S7 and S8 of the supplementary data, respectively. The On-X valve exhibited the most similar values in jet velocity, followed by the HP and CM valves. While HP and On-X valves exhibited similar velocities, the CM valve displayed higher velocity values due to its smaller geometric orifice area and leaflet opening angle. Regarding vortex structures, $\lambda_2$ color maps and swirling strength iso-surfaces highlight MHV vortex shedding and indicate that the CM valve exhibited a vorticity budget at peak systole richer than HP and On-X valves.

The volume-averaged (distal to the sinotubular junction) values of swirling strength and stretching along the cardiac cycle are presented in figure 5 (see figure S9 in the supplementary data for averages over the entire fluid domain). For all MHVs, swirling strength and stretching increased rapidly during early flow deceleration, reaching a peak, and then gradually decreased during late flow deceleration and MHV closure. Regardless of the MHV model, stretching peak value occurred earlier than the swirling strength peak value, highlighting that vortices were shed by MHV leaflets, elongated in the fluid domain, and subsequently increased their swirling rate. The CM valve presented the highest peak values, followed by the On-X and HP valves. Since flow-rate oscillations at closure artificially impacted on diastolic vorticity transport, time-averaged swirling strength and stretching were compared among the three valves

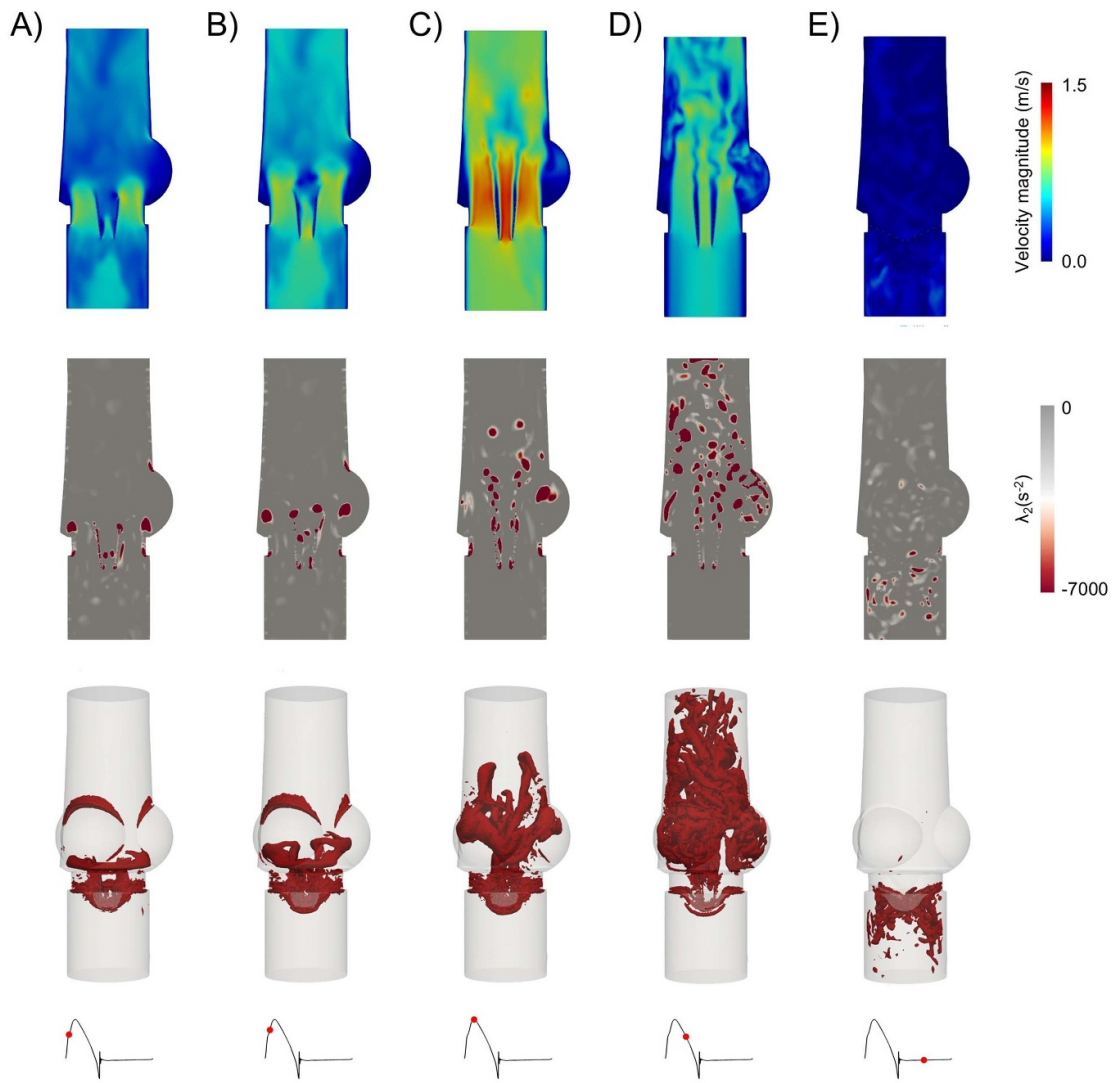


**Figure 3.** Hemodynamics of the Hemodynamic Plus valve: velocity magnitude and $\lambda_2$ color maps on a longitudinal section of the model and swirling strength iso-surfaces (swirling strength 80 $s^{-1}$) for the simulation replicating Nobili *et al* (2008) (Hemodynamic Plus valve in the straight aortic model) at five different time instants of the cardiac cycle: (A) and (B) during flow acceleration, (C) at peak systole, (D) during flow deceleration and (E) during diastole. For enhanced visualization, only the central portion of the domain is displayed.

**Table 1.** Cardiac output (CO) for the three mechanical heart valves assembled with the three aortic models.

| | CO (l $min^{-1}$) | | |
|---|---|---|---|
| | Straight | CU1 | CU2 |
| HP valve | 4.62 | 4.23 | 4.28 |
| On-X valve | 4.41 | 4.06 | 4.14 |
| CM valve | 3.44 | 3.57 | 3.34 |

CO: cardiac output; CU1: curved aortic model 1; CU2: curved aortic model 2;
HP: Hemodynamic Plus; CM: Carbomedics Standard.

only over the systole (figure 5(D)). Marked differences, reaching 41% for swirling strength and 133% for stretching, were observed between the HP and CM valves.

The AWCD was 0.50 for the On-X valve and 0.48 for the HP and CM valves, indicating a similar impact of MHV design on disrupting large-scale flow coherence distally (figure 6(A)). Additionally, the three devices exhibited similar EOA values (table 2).

### 3.3. Impact of aortic curvature on hemodynamics

The CO values for the simulations of the three MHVs assembled with the three aortic models are reported in table 1. For each valve, the CO varied minimally in the curved aortic models compared to the

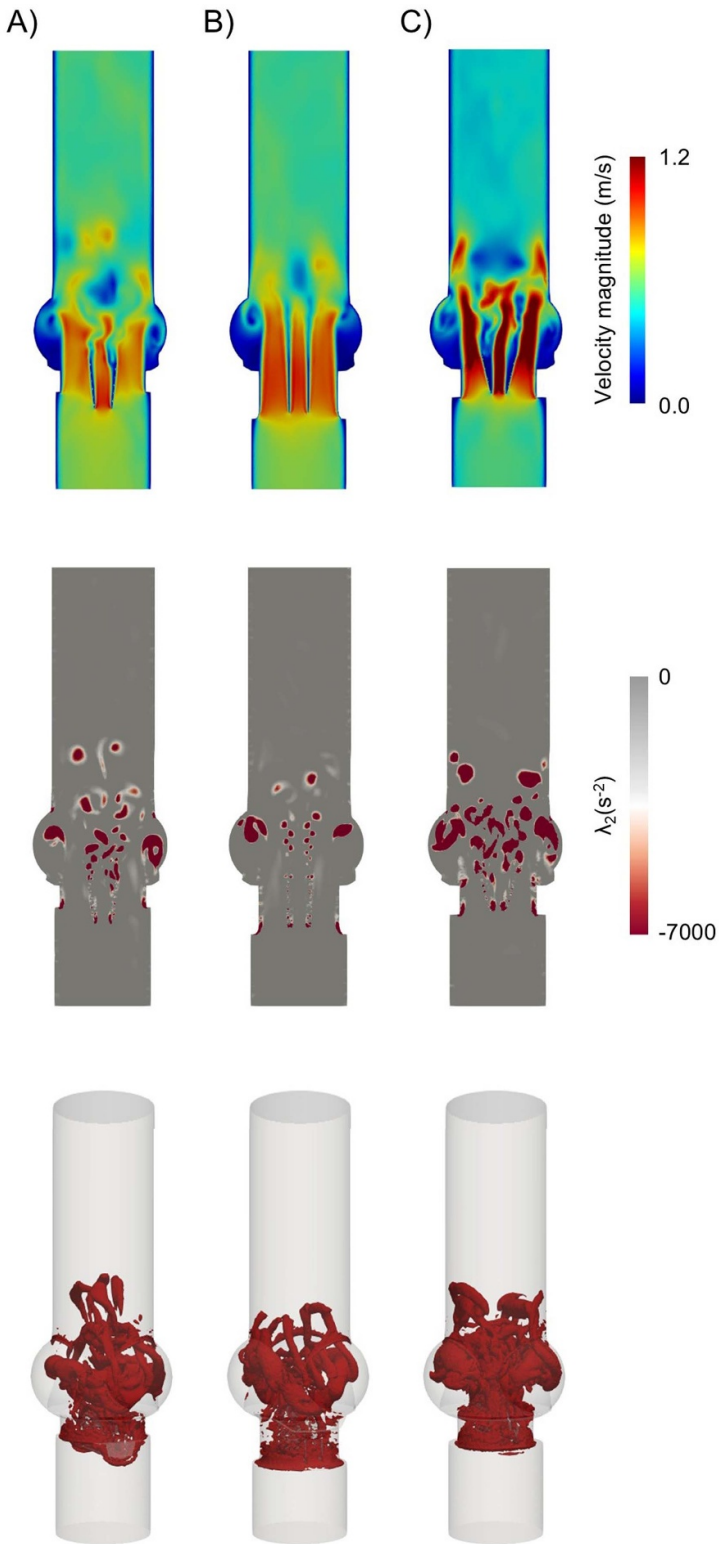


**Figure 4.** Impact of MHV design on hemodynamics: velocity magnitude and $\lambda_2$ color maps and swirling strength iso-surfaces (swirling strength $80\,s^{-1}$) at peak systole for the (A) Hemodynamic Plus (HP), (B) On-X and (C) Carbomedics Standard (CM) valves assembled with the straight aortic model. For enhanced visualization, only the central portion of the domain is displayed.

straight one, with percentage differences remaining below 10%. Color maps of velocity magnitude, $\lambda_2$ criterion and swirling strength iso-surfaces at peak systole for the three MHVs assembled with the three aortic models are shown in figures 7–9. For completeness, visualizations of velocity magnitude on axial cross-sections and of vorticity stretching are provided in figures S7 and S8 of the supplementary data, respectively. As expected, in both curved models, the flow field in the ascending aorta presented higher

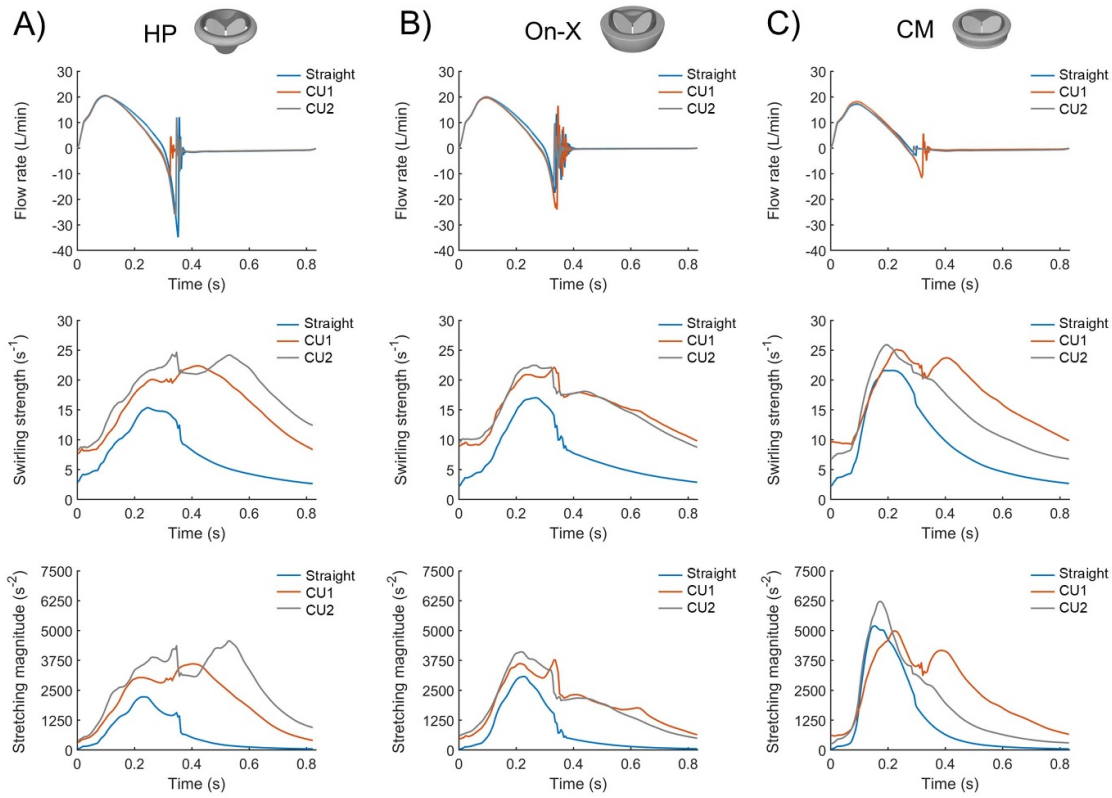


D)

| | Average systolic swirling strength ($s^{-1}$) | | |
|---|---|---|---|
| | Straight | CU1 | CU2 |
| HP valve | 9.8 | 13.6 | 15.3 |
| On-X valve | 10.2 | 14.7 | 15.7 |
| CM valve | 13.8 | 16.6 | 17.2 |

| | Average systolic stretching magnitude ($s^{-2}$) | | |
|---|---|---|---|
| | Straight | CU1 | CU2 |
| HP valve | 1203 | 1861 | 2301 |
| On-X valve | 1588 | 2151 | 2470 |
| CM valve | 2808 | 2813 | 3312 |

**Figure 5.** Impact of MHV design and aortic curvature on swirling strength and stretching: temporal evolution over the cardiac cycle of flow rate, average swirling strength and average vortex stretching for the (A) Hemodynamic Plus (HP), (B) On-X and (C) Carbomedics Standard (CM) valves assembled with the straight aortic model, curved model 1 (CU1), and curved model 2 (CU2); (D) average swirling strength and average vortex stretching during systole for the nine simulations. Averaged quantities are calculated downstream of the sinutubular junction.

velocity values on the intrados, partly ascribable to the presence of the near-wall MHV lateral jet generated by the valve's side orifice. Furthermore, aortic curvature had some impact on the swirling strength, which was dependent on the valve model. In the cases simulated in this study, the lateral valve jet interacted with the aortic wall at the intrados (giving rise to an increase in vorticity caused by the interaction between flow separation at the curvature and the resulting shear layer effects) only for the HP and CM valves with CU2 aortic model (figures 7(C) and 9(C)).

From a quantitative perspective, the simulations with curved aortic models revealed higher volume-averaged swirling strength and stretching in the vorticity field compared to the straight aortic model, irrespective of MHV design (figures 5(A)–(C)). This can be attributed to the vortex structures generated by the aortic curvature and to their potential interaction with the vortices shed by the MHV. Specifically, aortic curvature is known to contribute to the generation of counter-rotating, large-scale, helical fluid structures that mitigate transition to turbulence (Morbiducci *et al* 2009b, 2011, Dyverfeldt *et al* 2023). These helically shaped structures interact with the vortex structures generated by MHVs in different ways, depending on valve design and aortic curvature profile. During flow acceleration and early flow deceleration, a higher arch height-to-width ratio was associated with higher swirling strength and stretching for all the three MHV designs. Swirling strength and stretching at closed MHV exhibited similar values in the two curved aortic models for the On-X valve, while higher values were observed for the HP valve in CU2 model and for the CM valve in the CU1 model. As the flow-rate oscillations

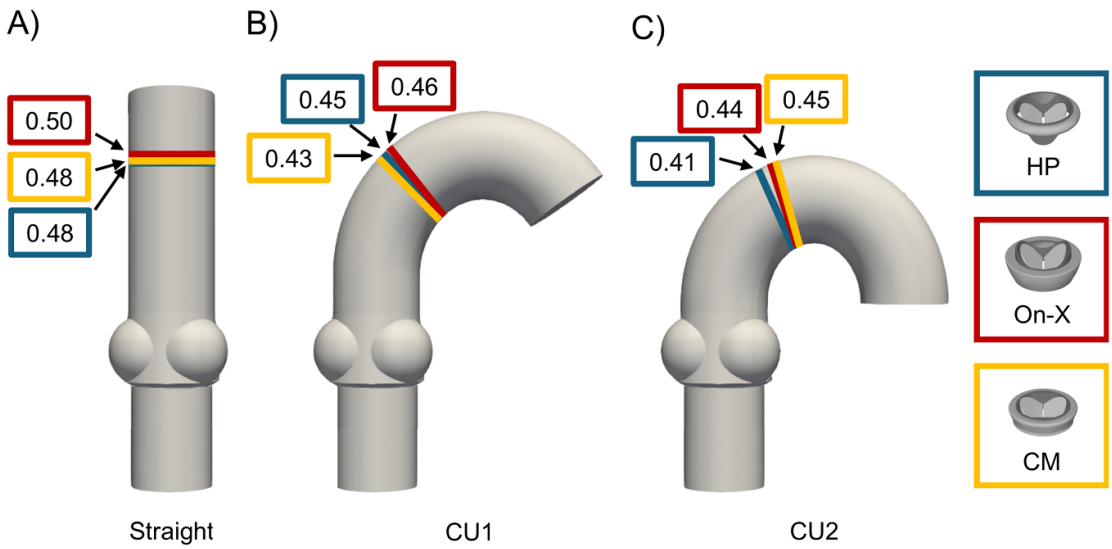


**Figure 6.** Impact of MHV design and aortic curvature on large-scale hemodynamic coherence: average weighted curvilinear distance (AWCD) for the Hemodynamic Plus (HP), On-X and Carbomedics Standard (CM) valves assembled with (A) straight aortic model, (B) curved model 1 (CU1) and (C) curved model 2 (CU2). For enhanced visualization, only a portion of the ventricular conduit and of the straight aortic conduit is displayed.

**Table 2.** Effective orifice area (EOA) for the three mechanical heart valves assembled with the three aortic models.

| | EOA ($cm^2$) | | |
|---|---|---|---|
| | Straight | CU1 | CU2 |
| HP valve | 1.71 | 1.74 | 1.74 |
| On-X valve | 1.67 | 1.67 | 1.69 |
| CM valve | 1.49 | 1.57 | 1.51 |

EOA: effective orifice area; CU1: curved aortic model 1; CU2: curved aortic model 2; HP: hemodynamic plus; CM: Carbomedics Standard.

affecting valve closure might have hampered the reliability of results in the diastolic phase, the following quantitative analysis focused on the systole only. Differences between the straight aortic model and the CU2 model reached up to 56% for average systolic swirling strength and 91% for average systolic stretching (figure 5(D)).

Aortic curvature determined moderately lower AWCD compared to the straight models for the three MHV designs (figure 6). In detail, the three MHV designs induced very similar AWCD values when implanted in the same aortic model (in the range 0.43–0.46 for CU1, 0.41–0.45 for CU2), with our findings suggesting that aortic curvature has a greater impact on large-scale flow coherence disruption than valve design.

EOA values are reported in table 2 and highlight a negligible impact of both MHV design and aortic curvature.

## 4. Discussion

Computational models can support the development phase of cardiovascular devices, and specifically of MHVs, by complementing and refining *in vitro* experimentation (Arminio *et al* 2024). In this study, an FSI framework for the *in silico* assessment of MHV performance was presented and applied to analyze the hemodynamics of MHVs with different designs in aortic models characterized by varying curvatures. The analysis focused on the transport of large-scale vorticity, encompassing both instantaneous visualizations and the integral quantification of vorticity field richness throughout the entire cardiac cycle, which has not been deeply examined in previous studies on MHVs (Arminio *et al* 2024).

The proposed FSI framework was evaluated by comparing its results with those from previous experimental and computational studies. Specifically, the simulation replicating a test performed on the HP valve using the ViVitro Pulse Duplicator system closely matched experimental measurements (Nobili *et al* 2008). The main difference observed from experimental data was the presence of oscillations in

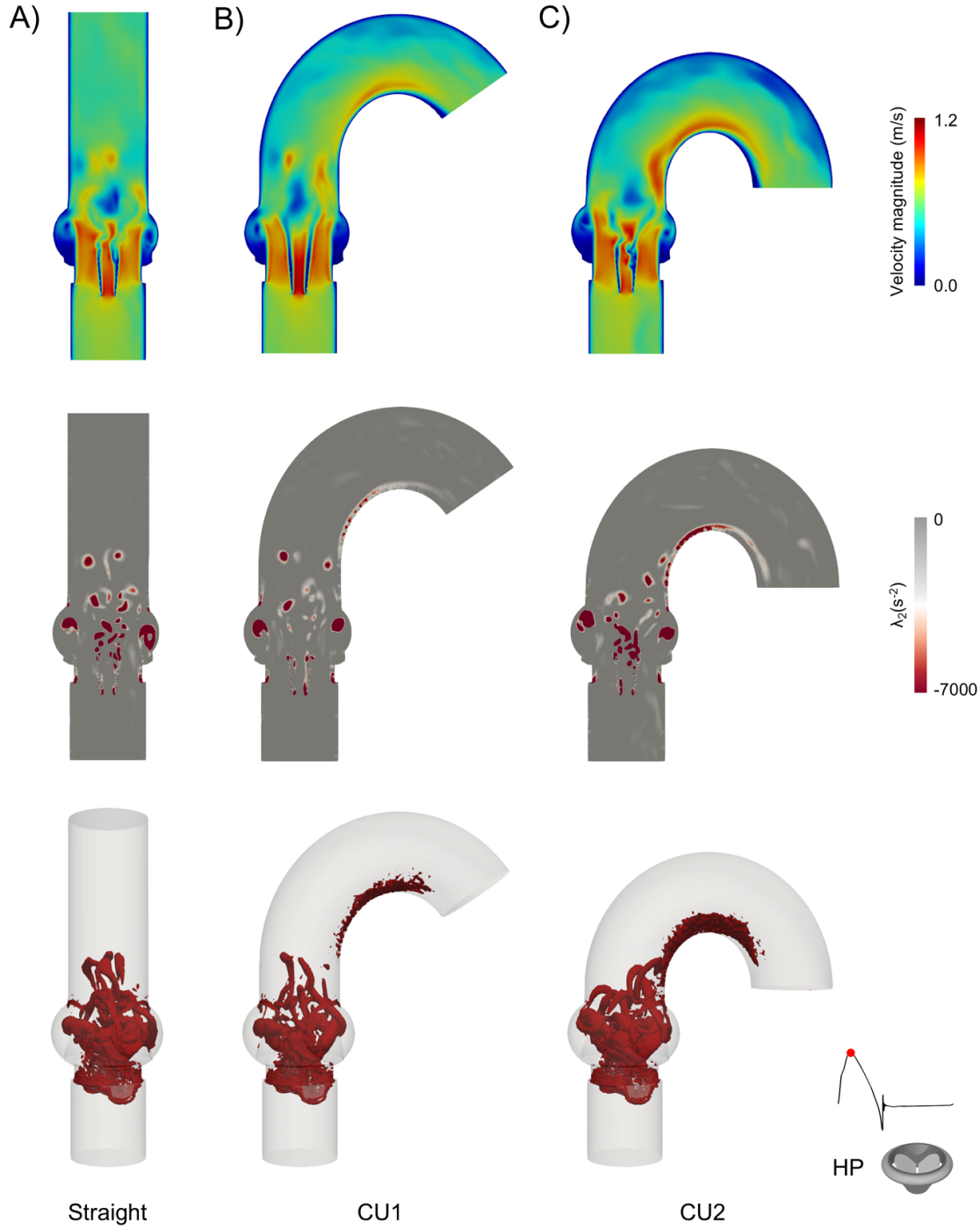


**Figure 7.** Impact of aortic curvature on Hemodynamic Plus (HP) valve hemodynamics: velocity magnitude and $\lambda_2$ color maps on a longitudinal section of the model and swirling strength iso-surfaces (swirling strength $80\,s^{-1}$) at peak systole for the HP valve assembled with (A) the straight aortic model, (B) curved model 1 (CU1), and (C) curved model 2 (CU2). For enhanced visualization, only a portion of the ventricular conduit and of the straight aortic conduit is displayed.

the FSI simulated flow-rate waveform during valve closure. This behavior was also reported in previous studies (Hsu *et al* 2014, Baylous *et al* 2024, Oliveira *et al* 2024), and can be attributed to two main factors: (i) the adoption of a Neumann boundary condition by prescribing a transvalvular pressure drop, which fails to fully capture the complexity of experimental set-ups that include components dampening flow-rate oscillations (Oliveira *et al* 2024); (ii) the rigid-wall assumption, which has been shown to amplify the intensity of flow-rate oscillations, compared to models with deformable walls (Hsu *et al* 2014). Additionally, the simulated velocity fields confirmed the well-known three-jet systolic flow pattern characteristic of bileaflet MHVs (Yoganathan *et al* 2004), with the predicted velocity magnitude color maps matching a previous study (Nobili *et al* 2008). The evolution of large-scale vortex structures in the aortic root showed good agreement with previous findings (Dasi *et al* 2007, Ge and Sotiropoulos 2007). Minor

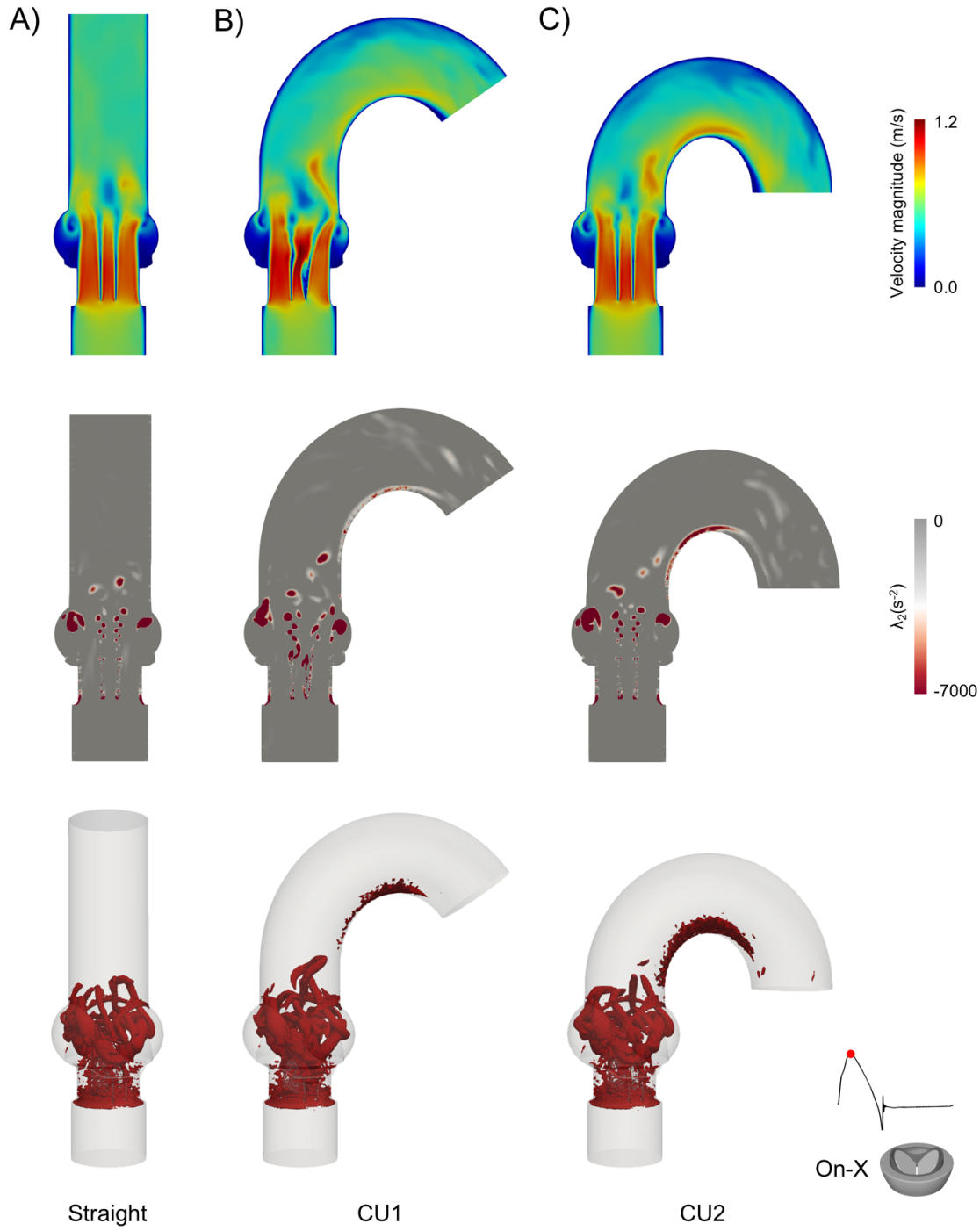


**Figure 8.** Impact of aortic curvature on On-X valve hemodynamics: velocity magnitude and $\lambda_2$ color maps on a longitudinal section of the model and swirling strength iso-surfaces (swirling strength $80\,s^{-1}$) at peak systole for the On-X valve assembled with (A) the straight aortic model, (B) curved model 1 (CU1), and (C) curved model 2 (CU2). For enhanced visualization, only a portion of the ventricular conduit and of the straight aortic conduit is displayed.

discrepancies were observed in the MHV region during diastole, likely due to an inhomogeneous activation of the gap closure feature.

The proposed FSI methodology is suited for investigating how MHV design influences large-scale hemodynamics. In this study, it was specifically used to analyze three different MHV designs resembling commercial valves commonly used in clinical practice, each featuring a distinct leaflet opening angle. The three MHVs exhibited differences in the shape and stability of their systolic flow jets. Specifically, the HP valve with its 85° leaflet opening angle exhibited limited boundary layer separation at leaflet surface, consistent with findings reported in the literature (Gross *et al* 1988). Differently, the CM valve promoted greater mixing in the distal flow field, with fluttering of the central flow jet (Gross *et al* 1988, King *et al* 1996). The On-X valve, featuring a 90° leaflet opening angle, encouraged more organized

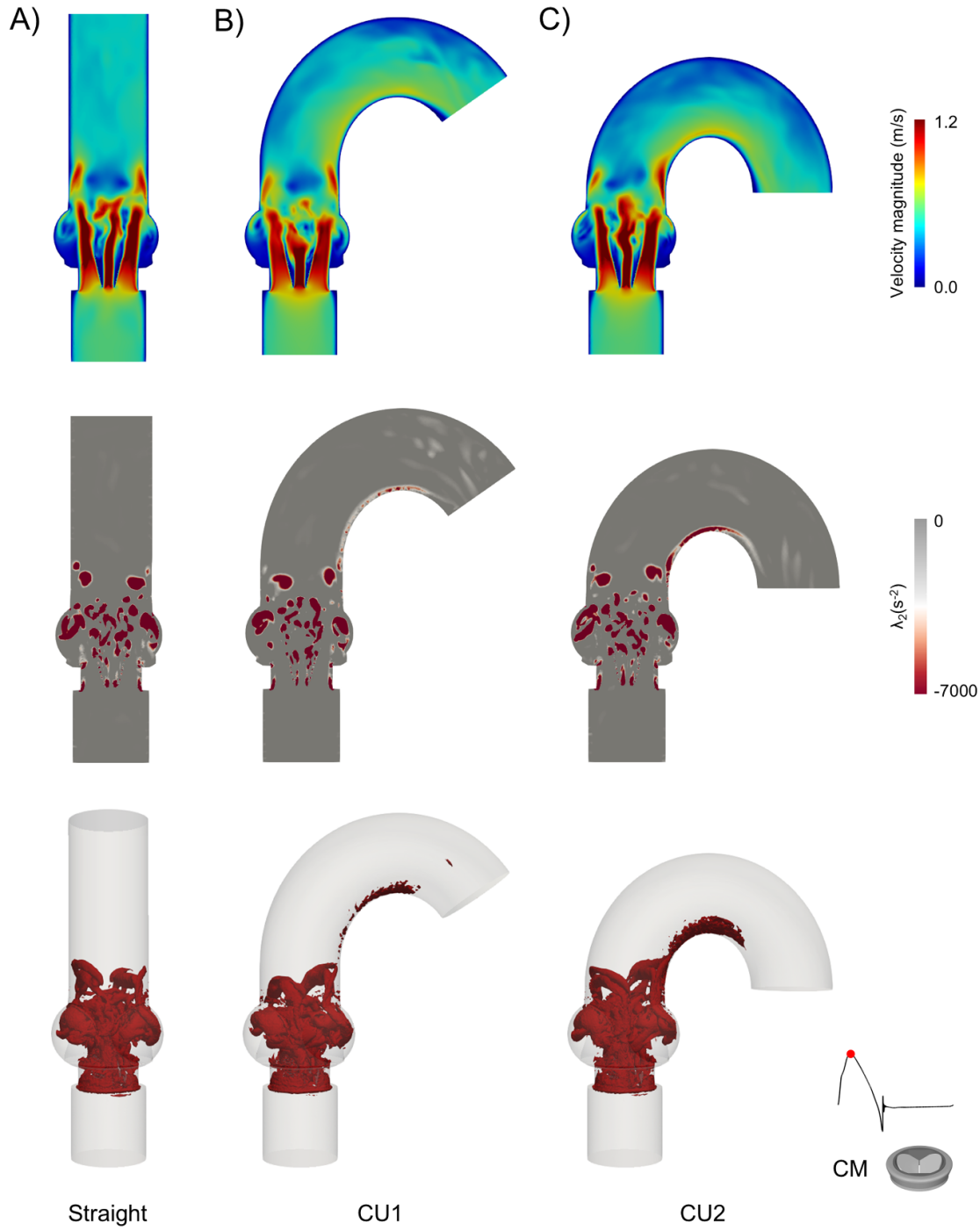


**Figure 9.** Impact of aortic curvature on Carbomedics Standard (CM) valve hemodynamics: velocity magnitude and $\lambda_2$ color maps on a longitudinal section of the model and swirling strength iso-surfaces (swirling strength $80s^{-1}$) at peak systole for the CM valve assembled with (A) the straight aortic model, (B) curved model 1 (CU1), and (C) curved model 2 (CU2). For enhanced visualization, only a portion of the ventricular conduit and of the straight aortic conduit is displayed.

flow patterns (Jawitz *et al* 2020). As previously reported (Lu *et al* 2004), the CM valve generated lateral jets that deviated from the axial flow direction, a hemodynamic feature that may alter tissue growth in regions where the jets impinge (King *et al* 1996). In contrast, the On-X valve produced symmetric, semi-circular lateral jets (figure S7) that were nearly aligned with the axial flow direction (Hatoum *et al* 2020, Ferrari and Obrist 2024). The HP valve exhibited an intermediate lateral jets orientation, falling between those of the CM and On-X valves.

The FSI approach proposed in this study also allowed for a detailed investigation of how aortic geometry affects hemodynamics, with a particular focus on the role of aortic curvature, which has not been systematically studied before. Although idealized aortic geometries were considered, the results suggest that the shape of the aorta has a minor impact on jet velocity immediately downstream of the MHV,

consistent with previous findings (Borazjani *et al* 2010). However, curved aortic models can result in different large-scale vorticity transport, with increased swirling strength and vorticity stretching compared to straight aortic conduits. This behavior arises from the combined effect of two factors: vorticity induced by aortic arch curvature and contribution given by the vortex structures generated by the MHV. While the individual contributions of these two mechanisms were not isolated, the distinct increases in swirling strength and vorticity stretching observed across the three MHVs in curved versus straight models suggest that the interaction between curvature-induced and MHV-generated vortices is influenced by the specific MHV design. This interaction is also likely affected by the rotational orientation of the MHV leaflets, which governs the alignment of lateral jets relative to the aortic arch. Since previous studies have highlighted a possible connection between large-scale vortex structures and mechanically-induced blood damage (Bluestein *et al* 2000, Morbiducci *et al* 2009a), the current findings on vorticity transport suggest that MHV hemodynamic performance tests should be extended to include aortic conduits with different curvature profiles. Additionally, the impact of the shape of the aorta was further explored by comparing the hemodynamics in two aortic curved models with different height-to-width ratio. The two different aortic models exhibited minimal differences in swirling strength and stretching of the vorticity field, suggesting that, within the examined range, variations in aortic arch height-to-width ratio may have a limited effect on MHV-related hemodynamics.

This study is subject to several limitations. The comparison of the proposed FSI framework with *in vitro* experiments was conducted for only one valve design in a straight aortic model and was limited to integral quantities, following a common practice in aortic MHV FSI research, which typically evaluates simulation reliability based on leaflet angular motion and flow velocity fields (Arminio *et al* 2024). Further validation is advisable, ideally through dedicated experiments involving particle image velocimetry to capture vorticity dynamics. Additionally, FSI simulations were conducted under the assumption of rigid aortic wall, a common approach in aortic MHV FSI studies. This idealization is based on earlier observations reporting that aortic compliance does not markedly impact on MHV leaflet kinematics (Nobili *et al* 2008) and flow-field pressure waveforms (Abbas *et al* 2025). Moreover, assuming aortic rigidity does not compromise the validity of the comparative analysis among different MHV designs and aortas with distinct curvature profiles. To simulate valve closure an artificial gap was introduced along leaflet edge. However, uneven activation of the gap closure feature during diastole led to artificial backflow, preventing realistic quantification of the regurgitant fraction. Another limitation stems from the use of Neumann conditions in terms of pressure drop prescribed between inflow and outflow sections, which did not allow direct control of the CO. As a result, the lengths of the aortic conduits had to be adjusted in both straight and curved aortic models to ensure identical peak flow rates under the same driving pressure drop. This boundary set-up also introduced flow oscillations following MHV closure, thereby impacting diastolic hemodynamics and complicating the analysis of flow patterns during this phase. Future work could address these issues by implementing a flow-rate inlet boundary condition combined with either a pressure-type or Windkessel-type outlet boundary condition. Lastly, this study focused on large-scale fluid structures only, without studying turbulence. In this regard, maximum and mean systolic Reynolds numbers for the nine simulation scenarios fall in the range 3470–4160 and 2120–2600, respectively. Therefore, the Taylor microscale, delimiting the inertial subrange of the flow and defined as $\lambda = D \cdot (10/Re)^{1/2}$, is in the order of 1.5 mm and 1.9 mm for the maximum and mean Reynolds numbers, respectively. This is more than twice the average cell size of the selected meshes (0.63 mm). Consequently, the selected mesh size allows for fully resolving the inertial subrange of the flow, despite not resolving small eddies down to the Kolmogorov scale. Specifically, resolving the Kolmogorov scale (0.06 mm and 0.09 mm for the maximum and mean Reynolds numbers, respectively) would require a tenfold decrease in mesh size, with a significant increase in computational costs. Such resolution would have been unjustified in the present study, since the proposed results analysis did not encompass the evaluation of turbulent quantities. Additionally, the adopted approach is suitable for investigating large-scale fluid structures, given that previous heart valve FSI studies (Baylous *et al* 2024, Oliveira *et al* 2024) showed that the VMS method with OSS offers sufficient accuracy for comparative analyses, particularly since MHV leaflet dynamics is governed by integral flow scales (Nobili *et al* 2008). Future work would explore small-scale flow features, incorporating turbulence in the FSI framework, such as through Large Eddy Simulation or Direct Numerical Simulation approaches.

Despite these limitations, the proposed FSI framework proved to be a reliable and efficient tool for investigating MHV hemodynamics, particularly to explore different scenarios under consistent working conditions. This framework can be expanded to evaluate MHV performance under different implantation positions and in pathological aortic geometries. For instance, testing various orientations would

help assess how MHV lateral jets interact with the curvature profile of the aorta. Additionally, the framework allows for the evaluation of different valve sizes and alternative designs, including trileaflet and prototype MHVs, as recently explored experimentally by Ferrari and Obrist (2024) and Goode *et al* (2024). Finally, the insights gained from these simulations could be deepened by integrating blood damage models, helping to clarify the complex relationship between flow dynamics and the thromboembolic potential of MHVs (Morbiducci *et al* 2009a).

## 5. Conclusions

This study presents a reliable FSI framework for the hemodynamic assessment of MHVs, which was used here to investigate the impact of both MHV design and aortic curvature profile on the hemodynamic performance of the device. The findings confirm that MHV hemodynamics is influenced by device design features. Specifically, larger leaflet opening angles lead to more organized flow patterns. Among the tested valves, the On-X demonstrated the highest level of systolic flow organization, while the CM valve showed the lowest. Additionally, aortic curvature was found to impact large-scale vorticity transport. Specifically, testing MHVs in straight aortic models may result in less realistic vorticity dynamics, quantified here in terms of swirling strength and vorticity stretching. This highlights the importance of evaluating these devices in curved aortic conduits, enabling a more accurate assessment of how aortic arch curvature influences valve performance. While significant differences were observed between straight and curved aortic models, no substantial differences emerged among the curved models with varying degrees of curvature. Nevertheless, testing MHVs in conduits with a range of representative curvatures could help address the need to evaluate their hemodynamic performance in the light of inter-subject anatomical variability.

## Acknowledgment

The authors acknowledge Alberto Morena, Professor Lorenzo Peroni and Professor Alessandro Scattina (Politecnico di Torino, Italy) for their support with the LS-DYNA software.

## Funding sources

Umberto Morbiducci was partially supported by the project NODES, which has received funding from the MUR—M4C2 1.5 of PNRR funded by the European Union—NextGenerationEU (GA No. ECS00000036).

## Conflict of interest

The authors declare that they have no conflict of interest.

## Ethical approval

Not required.

## Author contribution

**Mariachiara Arminio**: Conceptualization, Methodology, Validation, Formal analysis, Investigation, Writing—original draft, Writing—Review & Editing, Visualization; **Dario Carbonaro**: Methodology, Formal analysis, Writing—original draft, Writing—Review & Editing; **Valentina Mazzi**: Formal analysis, Writing—Review & Editing; **Karol Calò**: Formal analysis, Writing—Review & Editing; **Rodrigo Paz**: Methodology, Writing—Review & Editing, Software; **Facundo Del Pin**: Methodology, Writing—Review & Editing, Software; **Diego Gallo**: Methodology, Writing—Review & Editing, Supervision; **Umberto Morbiducci**: Conceptualization, Methodology, Writing—Review & Editing, Supervision, Funding acquisition; **Claudio Chiastra**: Conceptualization, Methodology, Writing—Review & Editing, Supervision, Project administration.

## ORCID iDs

Mariachiara Arminio 0009-0000-0906-8317
Dario Carbonaro 0009-0004-0807-4538

Valentina Mazzi 0000-0002-3242-265X
Karol Calò 0000-0002-6935-4021
Rodrigo Paz 0000-0001-6242-4288
Facundo Del Pin 0000-0003-1242-6650
Diego Gallo 0000-0002-7409-7111
Umberto Morbiducci 0000-0002-9854-1619
Claudio Chiastra 0000-0003-2070-6142

## References

Abbas S S, Asadi H and Borazjani I 2025 Closure dynamics of aortic mechanical heart valves versus bioprosthetic heart valves *J. Fluid Mech.* **1012** 3
Abbas S S, Nasif M S and Al-Waked R 2022 State-of-the-art numerical fluid–structure interaction methods for aortic and mitral heart valves simulations: a review *Simulation* **98** 3–34
Annerel S, Claessens T, Taelman L, Degroote J, Van Nooten G, Verdonck P, Segers P and Vierendeels J 2015 Influence of valve size, orientation and downstream geometry of an aortic BMHV on leaflet motion and clinically used valve performance parameters *Ann. Biomed. Eng.* **43** 1370–84
Arminio M, Carbonaro D, Morbiducci U, Gallo D and Chiastra C 2024 Fluid-structure interaction simulation of mechanical aortic valves: a narrative review exploring its role in total product life cycle *Front. Med. Technol.* **6** 1399729
Baylous K, Kovarovic B, Paz R R, Anam S, Helbock R, Horner M, Slepian M and Bluestein D 2024 Thrombogenic risk assessment of transcatheter prosthetic heart valves using a fluid-structure interaction approach *Comput. Methods Programs Biomed.* **257** 108469
Bazilevs Y, Calo V M, Cottrell J A, Hughes T J R, Reali A and Scovazzi G 2007 Variational multiscale residual-based turbulence modeling for large eddy simulation of incompressible flows *Comput. Methods Appl. Mech. Eng.* **197** 173–201
Bluestein D, Rambod E and Gharib M 2000 Vortex shedding as a mechanism for free emboli formation in mechanical heart valves *J. Biomech. Eng.* **122** 125–34
Borazjani I, Ge L and Sotiropoulos F 2010 High-resolution fluid-structure interaction simulations of flow through a bi-leaflet mechanical heart valve in an anatomic aorta *Ann. Biomed. Eng.* **38** 326–44
Calò K, Capellini K, De Nisco G, Mazzi V, Gasparotti E, Gallo D, Celi S and Morbiducci U 2023a Impact of wall displacements on the large-scale flow coherence in ascending aorta *J. Biomech.* **154** 111620
Calò K, Gallo D, Guala A, Lodi Rizzini M, Dux-Santoy L, Rodriguez-Palomares J, Scarsoglio S, Ridolfi L and Morbiducci U 2023b Network-based characterization of blood large-scale coherent motion in the healthy human aorta with 4D flow MRI *IEEE Trans. Biomed. Eng.* **70** 1095–104
Calò K, Guala A, Mazzi V, Lodi Rizzini M, Dux-Santoy L, Rodriguez-Palomares J, Scarsoglio S, Ridolfi L, Gallo D and Morbiducci U 2024 Pathophysiology of the ascending aorta: impact of dilation and valve phenotype on large-scale blood flow coherence detected by 4D flow MRI *Comput. Methods Programs Biomed.* **255** 108369
Codina R, Badia S, Baiges J and Principe J 2004 Variational multiscale methods in computational fluid dynamics *Encyclopedia of Computational Mechanics* (Wiley)
Conti C A, Votta E, Della Corte A, Del Viscovo L, Bancone C, Cotrufo M and Redaelli A 2010 Dynamic finite element analysis of the aortic root from MRI-derived parameters *Med. Eng. Phys.* **32** 212–21
Corso P and Obrist D 2024 On the role of aortic valve architecture for physiological hemodynamics and valve replacement, part I: flow configuration and vortex dynamics *Comput. Biol. Med.* **176** 108526
Dasi L P, Ge L, Simon H A, Sotiropoulos F and Yoganathan A P 2007 Vorticity dynamics of a bileaflet mechanical heart valve in an axisymmetric aorta *Phys. Fluids* **19** 067105
De Tullio M D, Cristallo A, Balaras E and Verzicco R 2009 Direct numerical simulation of the pulsatile flow through an aortic bileaflet mechanical heart valve *J. Fluid Mech.* **622** 259–90
Dyverfeldt P, Trenti C, Ziegler M, Bjarnegård N and Lindenberger M 2023 Helical flow in tortuous aortas and its relationship to turbulence: a whole-aorta 4D flow MRI study *Front. Cardiovasc. Med.* **10** 1124604
Ferrari L and Obrist D 2024 Comparison of hemodynamic performance, three-dimensional flow fields, and turbulence levels for three different heart valves at three different hemodynamic conditions *Ann. Biomed. Eng.* **52** 3196–207
Ge L and Sotiropoulos F 2007 A numerical method for solving the 3D unsteady incompressible Navier–Stokes equations in curvilinear domains with complex immersed boundaries *J. Comput. Phys.* **225** 1782–809
Goode D, Scotten L, Siegel R and Mohammadi H 2024 Can mechanical heart valves perform similarly to tissue valves? An *in vitro* study *J. Biomech.* **174** 112270
Gross J M, Shermer C D and Hwang N H C 1988 Vortex shedding in bileaflet heart valve prostheses *ASAIO Trans.* **34** 845–50
Hatoum H, Maureira P and Dasi L P 2020 A turbulence *in vitro* assessment of On-X and St Jude Medical prostheses *J. Thorac. Cardiovasc. Surg.* **159** 88–97
Head S J, Çelik M and Kappetein A P 2017 Mechanical versus bioprosthetic aortic valve replacement *Eur. Heart J.* **38** 2183–91
Hiltner E, Erinne I, Singh A, Chen C, Kassotis J, Russo M and Sethi A 2022 Contemporary trends and in-hospital outcomes of mechanical and bioprosthetic surgical aortic valve replacement in the United States *J. Card Surg.* **37** 1980–8
Hsu M C, Kamensky D, Bazilevs Y, Sacks M S and Hughes T J R 2014 Fluid–structure interaction analysis of bioprosthetic heart valves: significance of arterial wall deformation *Comput. Mech.* **54** 1055–71
Huang C-J, Del Pin F, Çaldichoury I and Paz R R 2021 New development of the gap closure feature in LS-DYNA ICFD *13th European LS-DYNA Conf.* (*Ulm, Germany*)
International Organization for Standardization 2021 *(EN) ISO* 5840:2021 *Cardiovascular implants—Cardiac valve prostheses* (BSI Standards Publication)
Jawitz O K *et al* 2020 Rationale and design of PROACT Xa: a randomized, multicenter, open-label, clinical trial to evaluate the efficacy and safety of apixaban versus warfarin in patients with a mechanical On-X Aortic Heart Valve *Am. Heart J.* **227** 91–99
Jeong J and Hussain F 1995 On the identification of a vortex *J. Fluid Mech.* **285** 69–94
King M J, Corden J, David T and Fisher J 1996 A three-dimensional, time-dependent analysis of flow through a bileaflet mechanical heart valve: comparison of experimental and numerical results *J. Biomech.* **29** 609–18

Kleine P, Scherer M, Abdel-Rahman U, Klesius A A, Ackermann H and Moritz A 2002 Effect of mechanical aortic valve orientation on coronary artery flow: comparison of tilting disc versus bileaflet prostheses in pigs *J. Thorac. Cardiovasc. Surg.* **124** 925–32

Kuan Y H, Kabinejadian F, Nguyen V-T, Su B, Yoganathan A P and Leo H L 2014 Comparison of hinge microflow fields of bileaflet mechanical heart valves implanted in different sinus shape and downstream geometry *Comput. Methods Biomech. Biomed. Eng.* **18** 1785–96

Lu P C, Liu J S, Huang R H, Lo C W, Lai H C and Hwang N H C 2004 The closing behavior of mechanical aortic heart valve prostheses *ASAIO J.* **50** 294–300

Morbiducci U, Ponzini R, Nobili M, Massai D, Montevecchi F M, Bluestein D and Redaelli A 2009a Blood damage safety of prosthetic heart valves. Shear-induced platelet activation and local flow dynamics: a fluid-structure interaction approach *J. Biomech.* **42** 1952–60

Morbiducci U, Ponzini R, Rizzo G, Cadioli M, Esposito A, De Cobelli F, Del Maschio A, Montevecchi F M and Redaelli A 2009b In vivo quantification of helical blood flow in human aorta by time-resolved three-dimensional cine phase contrast magnetic resonance imaging *Ann. Biomed. Eng.* **37** 516–31

Morbiducci U, Ponzini R, Rizzo G, Cadioli M, Esposito A, Montevecchi F M and Redaelli A 2011 Mechanistic insight into the physiological relevance of helical blood flow in the human aorta: an in vivo study *Biomech. Model. Mechanobiol.* **10** 339–55

Nobili M, Morbiducci U, Ponzini R, Del Gaudio C, Balducci A, Grigioni M, Montevecchi F M and Redaelli A 2008 Numerical simulation of the dynamics of a bileaflet prosthetic heart valve using a fluid-structure interaction approach *J. Biomech.* **41** 2539–50

Nobili M, Passoni G and Redaelli A 2007 Two fluid-structure approaches for 3D simulation of St. Jude Medical bileaflet valve opening *J. Appl. Biomater. Biomech.* **5** 49–59

Oliveira H L, Buscaglia G C, Paz R R, Del Pin F, Cuminato J A, Kerr M, McKee S, Stewart I W and Wheatley D J 2024 Three-dimensional fluid–structure interaction simulation of the Wheatley aortic valve *Int. J. Numer. Methods Biomed. Eng.* **40** e3792

Otto C M *et al* 2020 ACC/AHA guideline for the management of patients with valvular heart disease: executive summary *Circulation* **143** E35–71

Petitjeans P 2003 Stretching of a vortical structure: filaments of vorticity *Europhys. News* **34** 20–23

Redheuil A, Yu W C, Mousseaux E, Harouni A A, Kachenoura N, Wu C O, Bluemke D and Lima J A C 2011 Age-related changes in aortic arch geometry: relationship with proximal aortic function and left ventricular mass and remodeling *J. Am. Coll. Cardiol.* **58** 1262–70

Sadipour M, Hanafizadeh P, Sadeghy K and Sattari A 2020 Effect of aortic wall deformation with healthy and calcified annulus on hemodynamic performance of implanted On-X valve *Cardiovasc. Eng. Technol.* **11** 141–61

Sotiropoulos F and Borazjani I 2009 A review of state-of-the-art numerical methods for simulating flow through mechanical heart valves *Med. Biol. Eng. Comput.* **47** 245–56

Sotiropoulos F, Le T B and Gilmanov A 2016 Fluid mechanics of heart valves and their replacements *Annu. Rev. Fluid Mech.* **48** 259–83

Sugawara J, Hayashi K, Yokoi T and Tanaka H 2008 Age-associated elongation of the ascending aorta in adults *JACC Cardiovasc. Imaging* **1** 739–48

Wu C *et al* 2019 *In-vitro* pulsatile flow testing of prosthetic heart valves: a round-robin study by the ISO cardiac valves working group *Cardiovasc. Eng. Technol.* **10** 397–422

Yoganathan A P, He Z and Jones S C 2004 Fluid mechanics of heart valves *Annu. Rev. Biomed. Eng.* **6** 331–62

Zakaria M S, Ismail F, Tamagawa M, Aziz A F A, Wiriadidjaja S, Basri A A and Ahmad K A 2017 Review of numerical methods for simulation of mechanical heart valves and the potential for blood clotting *Med. Biol. Eng. Comput.* **55** 1519–48

Zhou J, Adrian R J, Balachandar S and Kendall T M 1999 Mechanisms for generating coherent packets of hairpin vortices in channel flow *J. Fluid Mech.* **387** 353–96

Zhou J, Li Y, Li T, Tian X, Xiong Y and Chen Y 2023 Analysis of the effect of thickness on the performance of polymeric heart valves *J. Funct. Biomater.* **14** 309